Aerosol Science and Technology

ISSN: 0278-6826 (Print) 1521-7388 (Online) Journal homepage: https://www.tandfonline.com/loi/uast20

Counting efficiency determination from quantitative intercomparison between expansion and laminar flow type condensation particle counter

C. Tauber, G. Steiner & P. M. Winkler

To cite this article: C. Tauber, G. Steiner & P. M. Winkler (2019) Counting efficiency determination from quantitative intercomparison between expansion and laminar flow type condensation particle counter, Aerosol Science and Technology, 53:3, 344-354, DOI: 10.1080/02786826.2019.1568382

To link to this article: https://doi.org/10.1080/02786826.2019.1568382

AEROSOL SCIENCE AND TECHNOLOGY
2018, VOL. 53, NO. 3, 344–354
https://doi.org/10.1080/02786826.2019.1568382

Counting efficiency determination from quantitative intercomparison between expansion and laminar flow type condensation particle counter

C. Tauber[a], G. Steiner[a,b,c], and P. M. Winkler[a]

[a]Faculty of Physics, University of Vienna, Vienna, Austria; [b]Institute for Ion Physics and Applied Physics, University of Innsbruck, Innsbruck, Austria; [c]Grimm Aerosol Technik Ainring GmbH & Co Kg, Ainring, Germany

ABSTRACT

Heterogeneous nucleation of supersaturated *n*-butanol vapor on neutral silver particles of different size has been investigated at variable nucleation temperatures using a fast expansion chamber and a commercial continuous flow type condensation particle counter (CPC). In addition, the theoretical supersaturation profile was calculated for the commercial CPC in order to conflate the results with the measured onset saturation ratio of the expansion type size analyzing nuclei counter (SANC). A comparison of the experimental results of the SANC measurements with the Kelvin equation shows that the heterogeneous nucleation starts below the Kelvin curve. By introducing a correction factor for the Kelvin equation based on the SANC measurements, the theoretical detection efficiency for a laminar flow type CPC could be derived. It was the first time that a validation between theoretical saturation ratio profiles and measurements conducted with different methods to generate supersaturation was achieved. We made the observation that reducing the nucleation temperature generally leads to enhanced counting efficiencies. Consequently, the cutoff diameter of regular butanol CPCs can be significantly reduced by simply lowering the condenser temperature.

ARTICLE HISTORY
Received 27 August 2018
Accepted 2 January 2019

EDITOR
Jingkun Jiang

1. Introduction

The atmosphere contains a significant number concentration of aerosol particles, in heavily polluted environments sometimes up to $10^7 cm^{-3}$. The size of these particles ranges from a few nanometers up to around 100 μm. Only a small size fraction (in number concentration) is large enough to be visible, for example, cloud droplets, smoke or dust particles. Invisible smaller sized aerosol particles, however, constitute an important factor in cloud formation. Due to the fact that clouds are covering about 70% of the surface of our earth, aerosols play a significant role in shaping our climate (Stubenrauch et al. 2013). Nevertheless, the highest uncertainty in climate modeling is caused by cloud adjustment due to aerosols (IPCC 2013).

Atmospheric nano-particle formation by gas-to-particle conversion has been observed by measurements in the field. On a global scale it is seen as an important source controlling the number size distribution of atmospheric aerosols (Kulmala et al. 2004). Furthermore, it has been observed that these nano-particles can grow up to a size at which they can act as a cloud condensation nuclei (CCN) (Merikanto et al. 2009; Spracklen et al. 2008). As a consequence, aerosol nano-particles likely contribute to the indirect radiative forcing, thus influencing our climate (IPCC 2013). The number concentration of aerosol particles is typically measured using commercial Condensation Particle Counters (CPCs) (McMurry 2000). Most ultrafine continuous flow CPCs use *n*-butanol as working fluid and have typical lower particle detection limits in the range between 2.5 and 10 nm (Stolzenburg and McMurry 1991). *n*-butanol CPCs are operated at fixed temperatures of saturator and condenser. The performance towards the detection of even smaller particles may be optimized by choosing appropriate temperature settings.

In a recent paper by Barmpounis et al. (2018), it has been shown that by lowering the nucleation temperature in a butanol-based CPC the saturation ratio increases. To understand heterogeneous nucleation of

CONTACT C. Tauber christian.tauber@univie.ac.at Aerosol Physics and Environmental Physics, Faculty of Physics, University of Vienna, Boltzmanngasse 5, 1090 Vienna, Austria.
Color versions of one or more of the figures in the article can be found online at www.tandfonline.com/uast.
Supplemental data for this article is available online at on the publisher's website.

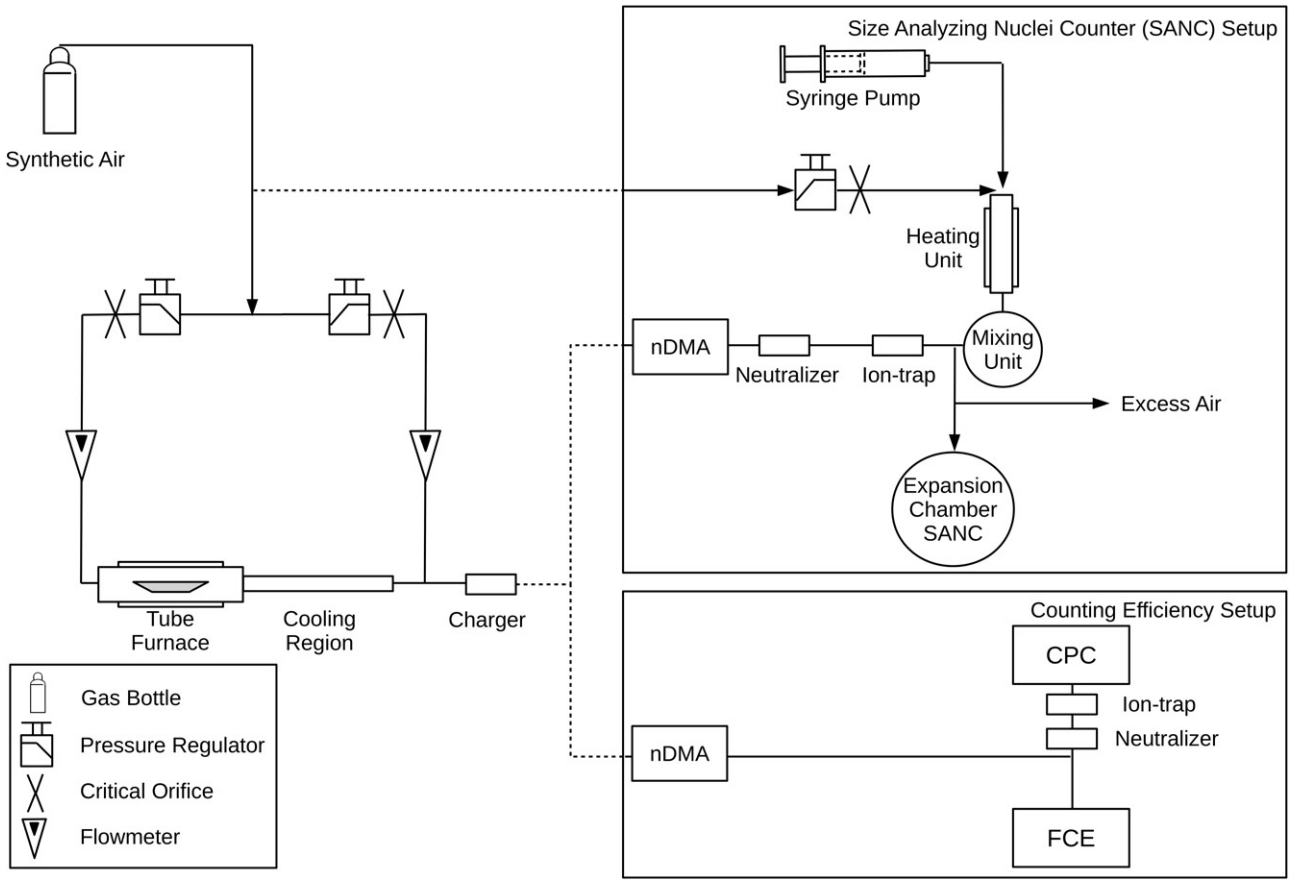

Figure 1. The experimental setup for evaluating the supersaturation and nucleation temperature with the SANC and the counting efficiency of a continuous flow type CPC, which was measured by operating a Faraday Cup Electrometer (FCE) in parallel.

n-butanol vapor on nano-particles in a size-range down to about 2 nm the temperature dependence was investigated in this work. This topic is worth examining since it gives information on the saturation ratio which is needed to activate particles in this size range. Results of earlier experiments with water vapor nucleating on silver nano-particles have shown an unusual temperature dependence (Kupc et al. 2013; McGraw, Winkler, and Wagner 2017). Further studies on the nucleation of *n*-propanol on sodium chloride particles in the temperature range from 262 to 287 K indicate a reversed trend of the onset saturation ratio compared to the Kelvin equation (Schobesberger et al. 2010). Due to the close chemical similarity of *n*-propanol and *n*-butanol, and the common use of *n*-butanol as a working fluid in commercial CPCs, the temperature dependence of heterogeneous nucleation of *n*-butanol on neutral silver (Ag) particles is investigated in this study. The generated Ag particles can be assumed to be spherical, insoluble and neutral. These prerequisites enable us to measure pure heterogeneous nucleation on spherical seeds (Winkler et al. 2016). Therefore temperature dependent expansion and laminar flow type CPC experiments were conducted. In addition, the supersaturation profile inside the condenser for an ultrafine CPC at different temperature settings was simulated. As a result, a quantitative intercomparison between the two different experimental approaches to activate nano-particles by vapor supersaturation can be established.

2. Materials and methods

2.1. Experimental

The experimental setup used for the expansion chamber and laminar flow type CPC is shown schematically in Figure 1. Ag particles were generated in a tube furnace (Scheibel and Porstendörfer 1983) which was supplied with synthetic air (ALPHAGAZ 1 AIR, $>=$ 99.999% (5.0), Air Liquide). For both set-ups, the polydisperse aerosol flow was kept constant at 3 L/min through the Americium 241 (Am-241) charger and the nano differential mobility analyzer (nDMA). By applying positive or negative voltage to the nDMA a monodisperse negatively or positively charged particle fraction can be selected. To rule out humidity effects, the relative humidity (RH) of the sheath air of the

nDMA was constantly measured with a sensor (HIH-4000-004, Honeywell). Thereby the accumulation of water in the silica gel dryer could be monitored. Before entering the SANC or the continuous flow type CPC the size selected silver particles were neutralized with a second Am-241 neutralizer.

For the SANC experiments particles were subsequently mixed with *n*-butanol containing carrier gas flow of 5 L/min and led into the expansion chamber (Wagner et al. 2003). *n*-butanol vapor was added to the system by controlled injection from a syringe pump, followed by quantitative evaporation of the liquid beam in a heating unit (see Figure 1; Winkler et al. 2008a). The resulting well-defined and nearly saturated vapor–air mixture together with size selected, neutralized monodisperse seed particles from the nDMA were passed into the temperature controlled expansion chamber of the SANC. Vapor supersaturation was achieved by adiabatic expansion. The amount of supersaturation is determined by the nucleation temperature T_{nuc} which was calculated from Poisson's law based on the pressures before and after expansion and the chamber temperature. The number concentration of droplets nucleated on the seeds was measured with the Constant Angle Mie Scattering (CAMS) method (Wagner 1985). Radius and number concentration of the growing droplets could thus be determined simultaneously. Neutralizer ions and the charged particles were removed by an ion-trap which was set to ±500 V. The capturing efficiency of the electrostatic precipitator was found to be >99% in the size-range between 1 and 10 nm. By varying the chamber temperature and the pressure drop in the expansion chamber, heterogeneous nucleation of *n*-butanol at nucleation temperatures ranging from 270 to 292 K was analyzed. The nucleation or activation probabilities using the SANC/CAMS method can be expressed as:

$$P = \frac{N_{\mathrm{activated}}}{N_{\mathrm{total}}} = 1 - \exp(-Jt). \tag{1}$$

Here, J is the heterogeneous nucleation rate and t is the time for activation. The total number concentration N_{total} of the monodisperse seeds was measured by conducting several experiments at saturation ratios significantly above the onset saturation ratio for each nucleation temperature. Thereby the stability of the aerosol concentration and the total number concentration could be monitored. We define the onset conditions as the saturation ratio S_0 when the nucleation probability reaches the value $P = 0.5$. The nucleation probability $P(S)$ at S_0 has the form of a cumulative Gumbel distribution (Winkler et al. 2016):

$$P(S) = 1 - \exp\left(-\exp\left(\ln(\ln 2) + (n^* + 1)(\ln S - \ln S_0)\right)\right). \tag{2}$$

By applying this form of distribution as a two-parameter fit function to the experimental data, the parameters n^* (number of molecules in the critical cluster) and S_0 could be evaluated. The resulting onset saturation ratio depending on the nucleation temperature was compared to Kelvin prediction.

In addition to the SANC measurements, the counting efficiency of an ultrafine continuous flow CPC (Model UCPC 3776, TSI Inc., Minneapolis, MN, USA) was measured at varied temperature settings of 18 degrees Kelvin at fixed ΔT. In contrast to the SANC experiments, the supersaturation is achieved by saturating the sheath flow and subsequently cooling the aerosol together with the saturated sheath flow in the condenser. In both methods the butanol vapor condenses, due to the decrease of temperature, on the aerosol and thereby increases the size of the particles. Accordingly, the particles grow to be micrometer sized and were thereby large enough to be counted by measuring the scattered light with a photodetector.

To determine the counting efficiency the neutralized aerosol was passed to the CPC and the charged one was passed to the Faraday cup electrometer (FCE) (Model 3068B Aerosol Electrometer, TSI Inc.), which was operated in parallel.

In order to calculate the counting efficiency of the neutralized aerosol, we evaluated the charging efficiency of the Americium-241 bipolar charger by using the Wiedensohler approximation (Wiedensohler 1988). Furthermore, the theoretical penetration efficiency was calculated for the measured size range based on Gormley and Kennedy (1948) and Wimmer et al. (2013) for FCE and CPC. To determine the detection efficiency η of a UCPC, the measured number concentration N_{CPC} of the CPC and the total number concentration N_{FCE} will be compared as follows:

$$\eta = \frac{N_{\mathrm{CPC}}}{N_{\mathrm{FCE}}}. \tag{3}$$

The particle detection efficiency depends mainly on the activation probability which is primarily a function of supersaturation and particle diameter (Barmpounis et al. 2018).

2.2. Simulation

To study the supersaturation profile of the ultrafine CPC, we developed a finite element model with FEniCS (Langtangen and Logg 2017). To include the

Table 1. Simulation parameter for the temperature and vapor pressure profiles.

Settings	Low T (°C)	Standard T (°C)	High T (°C)	Low p_v (mbar)	Standard p_v (mbar)	High p_v (mbar)
Sheath flow	25.0	25.0	25.0	0.0	0.0	0.0
Capillary flow	25.0	30.0	37.0	0.0	0.0	0.0
Condenser	1.1	10.0	18.9	1.4	2.9	5.5
saturator	30.1	39.0	47.9	13.1	23.6	41.0

0.05 L/min capillary flow in addition to the 0.25 L/min sheath flow in the simulation, a parabolic velocity flow profile was considered as input. A schematic layout of the flow pattern and a detailed description of the simulation parameter can be found in the supplementary information (SI). In the simulation convective as well as diffusive heat and mass transfer were considered to obtain temperature and vapor pressure profiles. The resulting profiles were used to calculate the saturation profile throughout the whole simulation domain. To solve the heat and mass transfer equations a fully developed laminar flow was assumed with no mixing of aerosol and sheath air flow (Stolzenburg and McMurry 1991). Thereby, the partial differential equation could be written as the so called Graetz problem (Eckert and Drake 1972). By transforming the original geometry to a circular tube we solved the problem with constant wall temperatures as follows (Eckert and Drake 1972; Schiesser and Silebi 1997; Stolzenburg and McMurry 1991):

$$P_e v(r) T_z = T_{rr} + \frac{1}{r} T_r + T_{zz}, \tag{4}$$

where $P_e = v_{\text{avg}} r_0/\alpha$ is the Peclet number, $v(r) = 2(1-r^2)$ is the parabolic flow velocity profile, v_{avg} is the average flow velocity, r_0 is the tube radius and α is the thermal diffusivity at the inlet of the simulation. The subscript notation denotes the partial derivative in r- and z-direction (Schiesser and Silebi 1997). The boundary conditions were assumed to be constant in the saturator and condenser for the partial vapor pressure of n-butanol p_v (perfectly wetted walls) and for the temperature T. All input parameters for the three different simulation settings are listed in Table 1 and the SI.

The introduced Peclet numbers for axial thermal diffusion ($P_{e,t} = 64$) and vapor ($P_{e,v} = 170$) from Stolzenburg and McMurry (1991) were used for the simulation. Thereby the thermal diffusion of the carrier gas and the diffusion of the vapor molecules can be computed. With the resulting profiles the saturation ratio profile inside the continuous flow type CPC was calculated as follows:

$$S = \frac{p_v}{p_{\text{sat}}(T)}, \tag{5}$$

where p_v is partial vapor pressure and $p_{\text{sat}}(T)$ is the temperature dependent saturation vapor pressure for n-butanol. This way we were able to estimate the supersaturation profile inside the condenser tube and together with the Kelvin equation we calculated the theoretical activation curve as shown in Stolzenburg and McMurry (1991). These simulations enabled us to combine our measured saturation ratio from the SANC with the counting efficiency measurements of the CPC. Accordingly an intercomparison between two measurement instruments using completely different methods of supersaturation generation becomes possible.

3. Results and discussion

We have measured the onset saturation ratio of n-butanol depending on nucleation temperature with the size analyzing nuclei counter SANC (Wagner et al. 2003; Tauber et al. 2018). In addition, the counting efficiency at variable condenser temperature, but constant ΔT between saturator and condenser, for a commercial n-butanol CPC was determined. With the SANC, heterogeneous nucleation probability (P) for different neutral Ag seeds in the size range of 2.5–9.0 nm mobility diameter was determined.

The experimental droplet growth rates for a spherical n-butanol droplet are determined from a one-to-one correspondence of experimental and theoretical (Mie) scattered light fluxes under a constant angle. The saturation ratio is verified from the comparison of experimental droplet growth curves to growth curves from a condensation model. As a result, the saturation ratio can be verified by an accuracy of 2–3%. Different saturation ratios and nucleation temperatures can be measured by varying the pressure drop in the expansion chamber. Due to the fast pressure reduction the temperature in the chamber is decreased, followed by nucleation and condensation. Hence the activation probability, as shown in Figure 2, which represents the fraction of activated particles vs. saturation ratio, can be measured. By adjusting the expansion chamber temperature, n-butanol vapor amount and the pressure drop these measurements can be done for different nucleation temperatures. In Table 2 all results for the different monodisperse

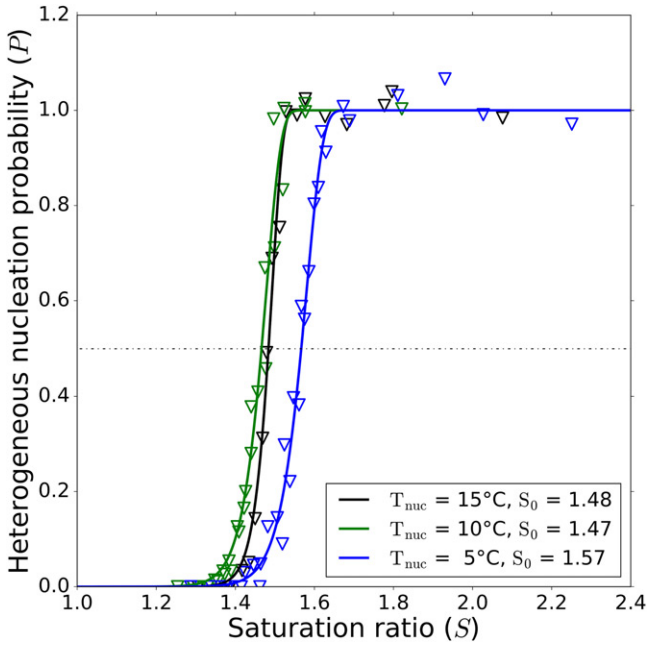

Figure 2. Heterogeneous nucleation probability of *n*-butanol on neutral silver seeds with mobility equivalent diameter of 6.5 nm at different nucleation temperatures. In this case, lower nucleation temperature coincides with higher saturation ratios needed for particle activation.

Table 2. SANC experimental results for the onset saturation ratio and the corresponding nucleation temperature for different monodisperse neutral silver seeds.

D_p (nm)	σ_g	S_0	T_{nuc} T (°C)	S_0	T_{nuc} T (°C)	S_0	T_{nuc} T (°C)	S_0	T_{nuc} T (°C)
2.5	1.072	3.16	−3.5	3.10	0.0	2.94	5.3		
3.0	1.071	2.66	2.7	2.48	10.0				
3.5	1.066	2.36	3.8	2.33	11.1				
5.0	1.068	1.83	4.1	1.85	7.4	1.79	12.4	1.77	14.4
6.5	1.067	1.57	5.6	1.47	10.8	1.48	15.2		
9.0	1.066	1.29	7.5	1.34	11.2	1.29	16.1	1.34	19.0

D_p is the mean mobility equivalent diameter, σ_g the mean geometric standard deviation, S_0 the onset saturation ratio and T_{nuc} the nucleation temperature.

neutral silver seeds under different nucleation temperatures are listed. In general within the measurement uncertainties the temperature dependence follows the theoretical Kelvin prediction, where with decreasing temperature the onset saturation ratio increases.

The resulting onset saturation ratios for different monodisperse silver particles and the critical cluster diameter depending on macroscopic bulk properties of *n*-butanol are shown in Figure 3. The nanometer sized particles were classified according to their electrical mobility and compared to the classical Kelvin diameter for different nucleation temperatures as depicted in Figure 3.

However, our results show that the needed onset saturation ratio for neutral silver seeds in the observed size range is lower than the Kelvin theory prediction. This finding is in line with already published results from Winkler et al. (2008b) and Schobesberger et al. (2010) for *n*-propanol. According to Winkler et al. (2012), the nucleation barrier can be crossed by kinetic processes like heterogeneous or ion induced nucleation. By neutralizing the generated aerosol we rule out a charge dependence and thereby limit the acting kinetic processes to pure heterogeneous nucleation. To associate the measured S_0 to the corresponding equilibrium Kelvin diameter $D_{K,eq}$ we introduced the fit parameter k as follows:

$$D^k_{K,eq} = k \times D_{K,eq} = k \times \frac{4\ \sigma\ M_w}{\rho\ N_A\ k_B T \ln(S)}, \qquad (6)$$

where M_w, σ, and ρ are the molecular weight, surface tension and the liquid density of *n*-butanol, N_A is the Avogadro constant and k_B is the Boltzmann constant. The measured saturation ratios with nucleation temperatures close to the three different condenser temperatures were used to fit the data for low, standard

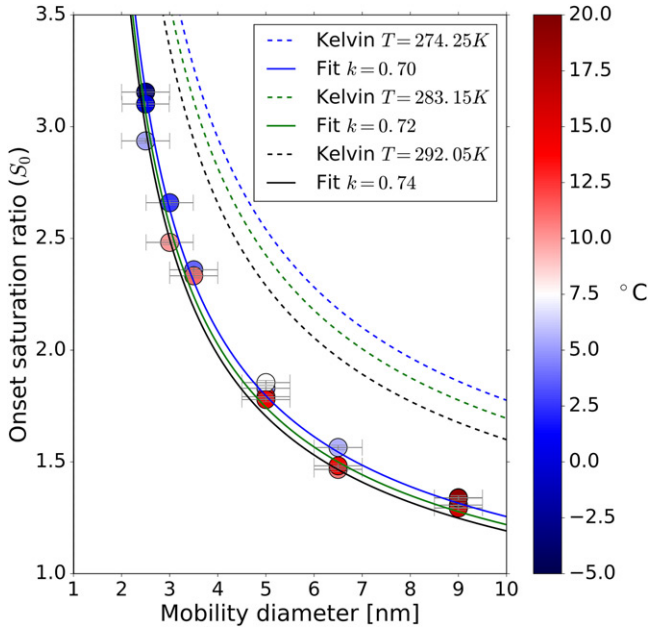

Figure 3. The onset saturation ratio versus mobility diameter for neutral Ag particles of different diameter: experimental data (colored dots), theoretical predictions according to Kelvin (dashed lines) and theoretical Kelvin prediction fitted to the measured data for the three different CPC temperature settings (low: blue line [$T = 274.25$K], standard: green line [$T = 283.15$K], high: black line [$T = 292.05$K]). The colorbar represents the temperature range in Celsius and the color of the dots corresponds to the measured nucleation temperature.

and high CPC settings (listed in Table 1). Thereby a value for k was found ranging from 0.70 to 0.74, which decreases the theoretical saturation ratio of the Kelvin equation.

By applying Equation (6) with the obtained correction factor k to our results of the modeled saturation ratio profile inside the continuous flow type CPC, we were able to calculate the theoretical activation curves for the TSI 3776 CPC at the applied three different temperature settings. Figure 4 shows the supersaturation profile for the three CPC settings. The decrease of the condenser and saturator temperature by about 9K (Figure 4a) from the default settings (Figure 4b) leads to an increase of the supersaturation ratio and vice versa as shown in Figure 4c. Therewith the corresponding diameter for $D_{p,0}$ and $D_{p,50}$ for 0 and 50% activation efficiency was determined. For $D_{p,0}$ the maximum of the centerline saturation ratio was used. This is shown in Figure 5a for the different CPC temperature settings. However, in a sheathed CPC the 50% activation diameter corresponds to the peak supersaturation and temperature along the flow trajectory that encompasses one-half of the flow. Therefore, the root mean square displacement of a particle with a diameter of 2.5 nm was calculated. This particle size corresponds to the theoretical cut-off diameter of a TSI 3776 UCPC. Then a range between the root mean square displacement at the inlet and outlet of the condenser for a 2.5 nm seed was defined, as explained in the SI. As a result, the corresponding maximum saturation ratio of the $D_{p,50}$ value range within a narrow band as shown in Figure 5b. This enables us to calculate the theoretical activation efficiency without using experimental data. The range also represents different diffusion coefficients for the three different temperature settings and for the varying particle sizes during the experiment. Together with Equation (6) the theoretical activation efficiency was derived as follows (Stolzenburg and McMurry 1991):

$$\eta_{act}(D_P) = 1 - \exp\left(-\log(2) \times (D_p - D_{p,0})/(D_{p,50} - D_{p,0})\right). \quad (7)$$

In Figure 5c the theoretical activation efficiencies for the three different temperature settings, calculated with the measured onset saturation ratio from the SANC for neutral silver seeds, are shown. To compare the theoretical activation curve to the measured counting efficiency, the charging and penetration losses must be considered.

Due to neutralization, the aerosol number concentration suffers a loss, which has to be taken into account for the comparison of the recorded particle concentrations. The particles removed by the electrical precipitator in front of the CPC reduce the counted total number concentration. This loss was calculated with the so called Wiedensohler approximation. Therewith the counted number concentration of the FCE was corrected to evaluate the neutral particle

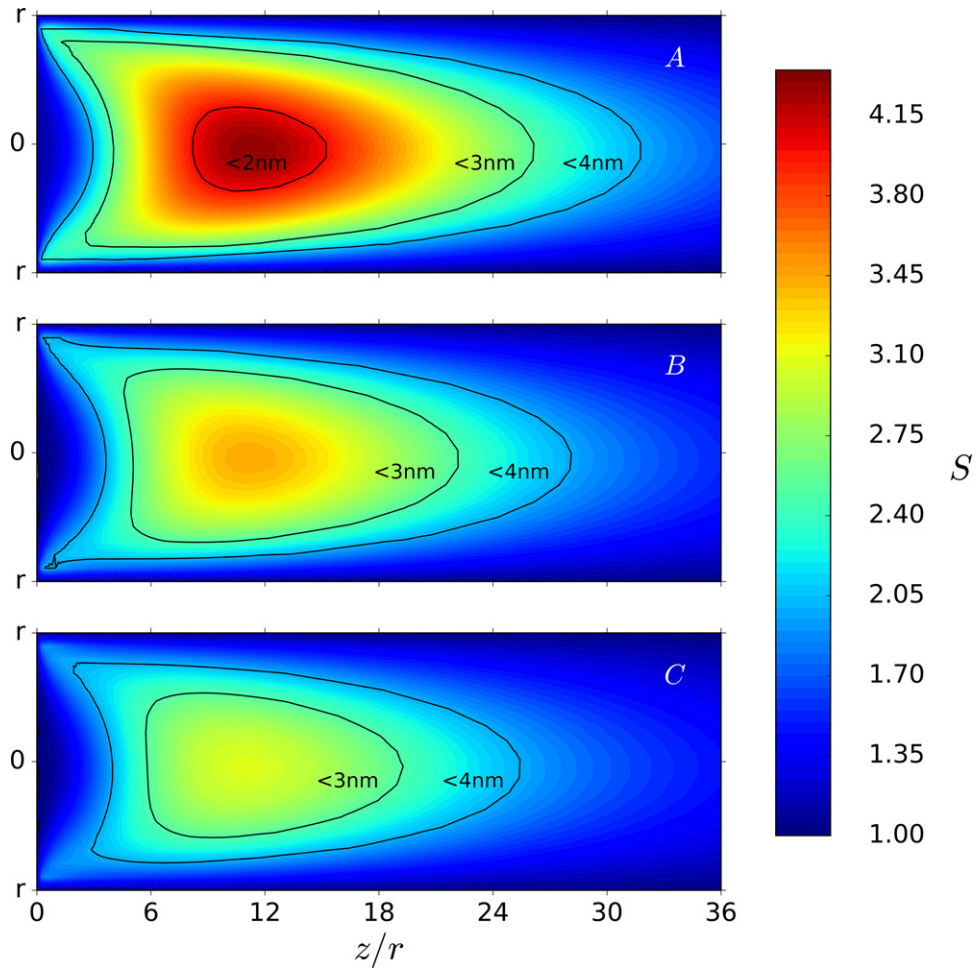

Figure 4. Supersaturation profiles for the condenser tube at low (a), standard (b) and high (c) temperature settings of the TSI 3776 CPC. r represents the radius of the condenser tube and z/r the dimensionless distance from the condenser inlet to the outlet. The color coding shows the propagation of the supersaturation profile inside the condenser tube. The black contour lines represent the calculated Kelvin diameter range based on the simulated saturation ratio.

fraction. The approximation is based on Fuchs theory (Fuchs et al. 1965) and describes the stationary state charge distribution of an aerosol after being exposed to the bipolar ionic atmosphere in the neutralizer. In this study we considered only singly charged silver seeds due to the small size of the test aerosol (<10 nm). The results of the theoretical penetration efficiency for the different CPC temperature settings can be found in the Figure S4. For the calculation an effective penetration length of 0.19 m for the CPC and 0.05 m for the FCE was used (Wimmer et al. 2013). The penetration efficiency of the CPC is almost independent of the actual temperature settings.

The inclusion of the charging and penetration efficiencies yields CPC detection efficiencies which are shown in Figure 6 and Table 3 for all temperature settings. Accordingly the theoretically and experimentally derived $D_{p,0}$ and cut-off diameter $D_{p,50}$ can be compared. Excellent agreement between the theoretical and the experimental $D_{p,0}$ of the CPC could be found. Hence, the maximum of the supersaturation profile could be reproduced with the applied model. However, the calculated cut-off diameter does not fit with the measured detection efficiencies for low and high T settings. This deviation could be a result of different diffusivity, because particles would exhibit higher diffusional losses to the condenser walls at high temperatures and vice versa. Consequently, the theoretical detection efficiency would shift for low T settings to smaller and for high temperatures to bigger diameters. As a consequence the deviation between measured and theoretical evaluated detection efficiency would decrease. The uncertainties during the detection efficiency measurements are mainly caused by the nDMA resolution and the particle detection accuracy of the FCE and CPC. In addition, the number concentration of the generated aerosol gets lower for particles below 2 nm mobility equivalent diameter and therefore accuracy suffers from low signal-to-noise ratios.

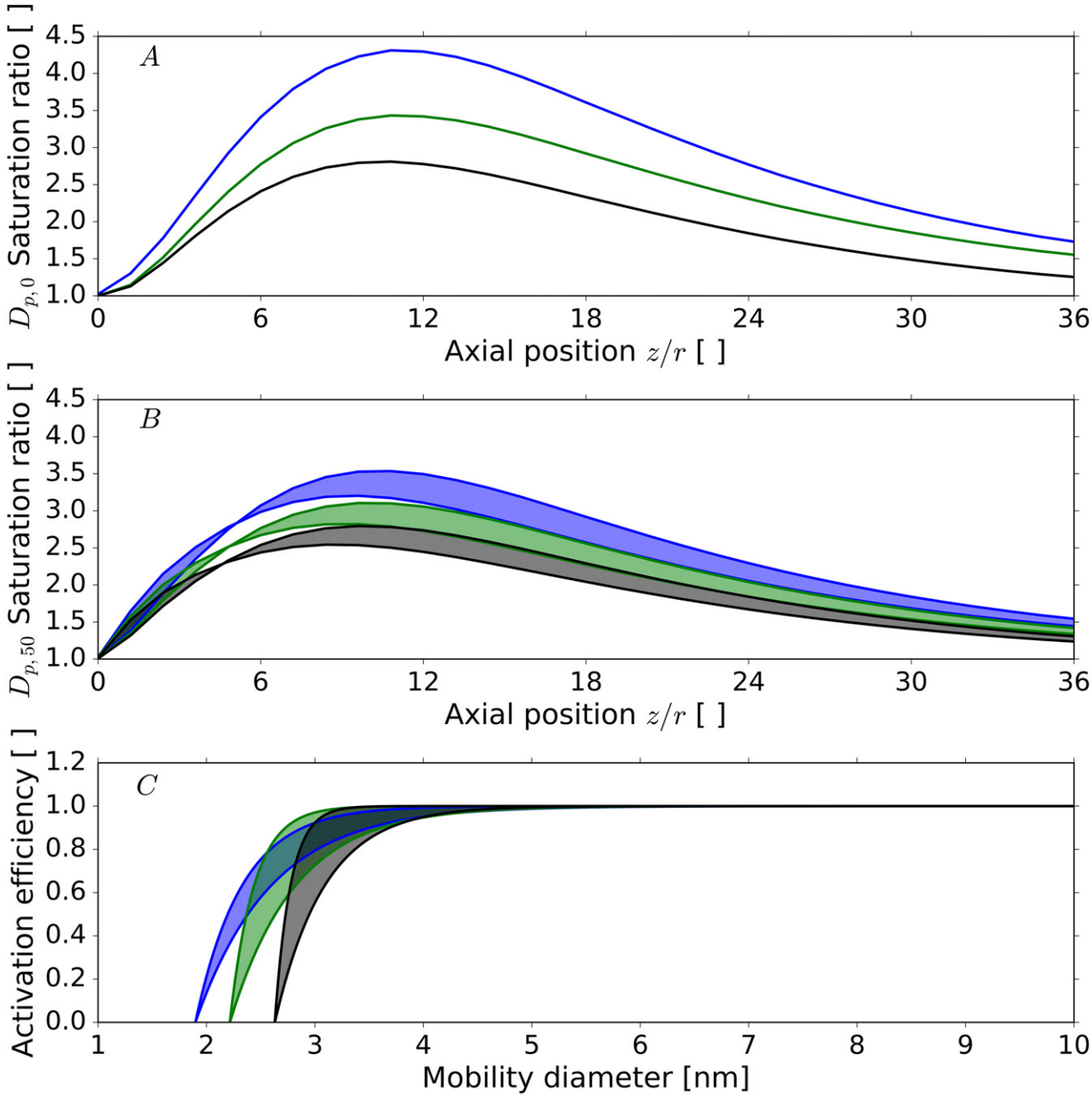

Figure 5. Theoretical calculation (a) of the centerline saturation ratio of *n*-butanol as function of dimensionless distance (z/r) from the simulation domain, (b) of the saturation ratio for the maximum and minimum root mean square displacement of a 2.5 nm particle traversing the condenser, (c) of the activation efficiency for the three different temperature settings (low: blue line, standard: green line, high: black line). The inner radius of the condenser tube was assumed to be $r = 2.3$ mm following Takegawa, Iida, and Sakurai (2017) and Stolzenburg and McMurry (1991). Diffusion and penetration losses were not considered in (c).

Since we applied positive (+) and negative (−) voltage for classification to the nDMA, we could also study the charging history. Before neutralizing the seeds, the particles are (+)- or (−)-charged, which has to be taken into account during the application of the Wiedensohler approximation. However, the charging history did not influence the counting efficiency measurements, and consistent with Kangasluoma et al. (2016), no sign preference for the neutralized aerosol with (+)- or (−)-charging history could be found. Figure 6 clearly illustrates that reduced temperature settings increase CPC counting efficiency and reduce the cut-off diameter.

4. Conclusion

The presented detection efficiency curves in this work were measured with a neutralized aerosol where

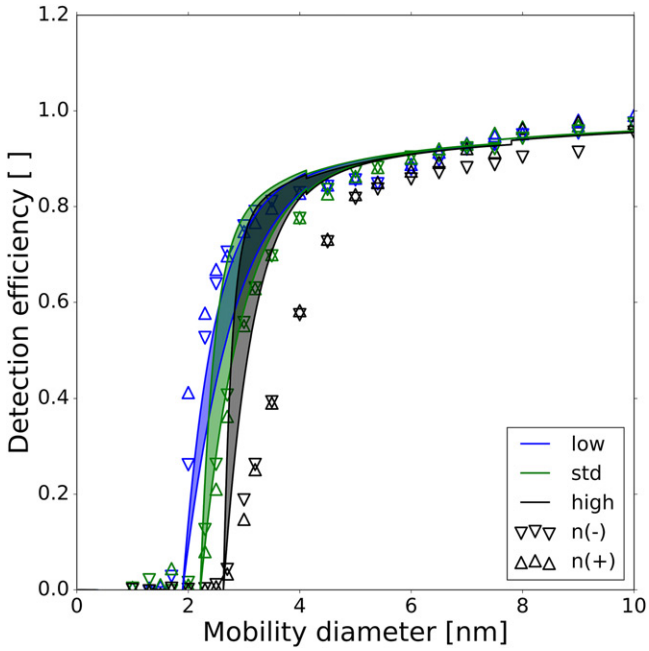

Figure 6. Theoretical detection efficiency of a TSI 3776 CPC for low, standard (std) and high temperature settings (lines). The triangles represent the measured counting efficiencies of neutralized positively or negatively charged seed particles. The shaded areas represent the resulting range of detection efficiency which was evaluated by considering the maximum and minimum root mean square displacement of a 2.5 nm particle inside the condenser.

Table 3. Theoretical and measured $D_{p,0}$ and $D_{p,50}$ cutoff diameter range for a TSI 3776 CPC at different temperature settings.

	Theoretical			Measurements		
T settings	Low	std	High	Low	std	High
$D_{p,0}$ [nm]	1.9	2.2	2.6	1.7	2.1	2.5
$D_{p,50}$ [nm]	[2.4, 2.6]	[2.5, 2.8]	[2.8, 3.0]	2.1	2.9	3.8

charge enhanced nucleation does not play a role. Within the uncertainties from the model and simulation study an intercomparison between an expansion type and a commercial continuous flow type CPC was made. The introduction of the fit parameter k allows to adopt the classical Kelvin diameter approach for comparing the different CPC types. It is the first time that we show in our studies that these different experimental approaches follow the same behavior as theoretical saturation ratio profile calculations. We also have shown that with precise nucleation probability measurements performed using the SANC the counting efficiencies of a continuous flow-type CPC can be predicted.

In summary, by lowering the operating temperature range by 9 K of a standard TSI 3776 UCPC and keeping ΔT between saturator and condenser constant, we could achieve a reduction of the cut-off diameter $(D_{p,50})$ from 2.9 nm to about 2.1 nm for the neutral aerosol composition. In contrast to Barmpounis et al. (2018), ΔT between saturator and condenser was not increased. The calculated saturation ratio profiles inside the condenser tube are not elevated by increasing ΔT, but due to the temperature reduction. There are two aspects which help to explain the increased saturation ratio as a result of lowered temperature settings. Firstly, it can be explained by the higher saturator to condenser vapor pressure ratio at low temperature which leads to an increased excess vapor amount above saturation vapor pressure in the condenser tube. Secondly, the simulated centerline temperature profiles for the saturator and saturator extension do not reach the preset saturator temperature as shown in the Figure S2. As a result, a higher temperature gradient at the condenser inlet for low CPC settings can be achieved. This also leads to an increase of the saturation ratio. During our measurements the saturation ratios were always significantly lower than the S_0 for homogeneous nucleation, which for *n*-butanol at these temperatures is between 5 and 6 (Viisanen and Strey 1994).

During the heterogeneous nucleation of *n*-butanol vapor onto neutral silver seeds no sign preferences for previously positively or negatively charged particles

were found. In this study special care was taken to reduce humidity, charge, and solubility effects. As a result by simply reducing the temperature settings of a UCPC we found a reduced cut-off diameter. Under ambient air conditions the resulting values may vary due to increased RH or different particle surfaces interactions. Previous studies conducted by Schobesberger et al. (2010) show that the nucleation of n-propanol vapor—which is chemically similar to *n*-butanol—onto sodium chloride nano-particles show an inverse temperature trend. In this case the cutoff diameter would even be lower for the low temperature settings of the CPC. In addition, increased RH in the carrier gas could lead to a binary heterogeneous nucleation. Therefore, further studies, including different seed and vapor properties, charging states and particle composition, are necessary for a better understanding of the driving processes behind heterogeneous nucleation.

Acknowledgment

We thank Peter Josef Wlasits for his help with the CPC characterizations.

Funding

This work was supported by the European Research Council under the European Community's Seventh Framework Programme (FP7/2007/2013)/ERC grant agreement no. 616075.

ORCID

C. Tauber http://orcid.org/0000-0003-1453-1067
G. Steiner http://orcid.org/0000-0003-3008-1414

References

Barmpounis, K., A. Ranjithkumar, A. Schmidt-Ott, M. Attoui, and G. Biskos. 2018. Enhancing the detection efficiency of condensation particle counters for Sub-2nm particles. *J. Aerosol Sci.* 117 :44–53. doi:10.1016/j.jaerosci.2017.12.005.

Eckert, E. R. G., and R. M. J. Drake. 1972. *Analysis of heat and mass transfer*. New York: McGraw-Hill.

Fuchs, N. A., R. E. Daisley, M. Fuchs, C. N. Davies, and M. E. Straumanis. 1965. The mechanics of aerosols. *Phys. Today* 18 (4):73. doi:10.1063/1.3047354.

Gormley, P. G., and M. Kennedy. 1948. Diffusion from a stream flowing through a cylindrical tube. *Proc. R. Irish Acad. Sect.A: Math. Phys. Sci.* 52 :163–169.

IPCC 2013. *Summary for policymakers*. book section SPM, pages 1–30. Cambridge, UK: Cambridge University Press.

Kangasluoma, J., A. Samodurov, M. Attoui, A. Franchin, H. Junninen, F. Korhonen, T. Kurten, H. Vehkamäki, M. Sipilä, K. Lehtipalo, D. R. Worsnop, T. Petäjä, and M. Kulmala. 2016. Heterogeneous nucleation onto ions and neutralized ions: Insights into sign-preference. *J. Phys. Chem. C* 120 (13):7444–7450. doi:10.1021/acs.jpcc.6b01779.

Kulmala, M., L. Laakso, K. E. J. Lehtinen, I. Riipinen, M. Dal Maso, T. Anttila, V.-M. Kerminen, U. Horrak, M. Vana, and H. Tammet. 2004. Initial steps of aerosol growth. *Atmos. Chem. Phys.* 4 (11/12):2553–2560. doi:10.5194/acp-4-2553-2004.

Kupc, A., P. M. Winkler, A. Vrtala, and P. E. Wagner. 2013. Unusual temperature dependence of heterogeneous nucleation of water vapor on ag particles. *Aerosol Sci. Technol.* 47 (9):i–iv. doi:10.1080/02786826.2013.810330.

Langtangen, H. P., and A. Logg. 2017. *Solving PDEs in python*. Cham: Springer.

McGraw, R. L., P. M. Winkler, and P. E. Wagner. 2017. Temperature dependence in heterogeneous nucleation with application to the direct determination of cluster energy on nearly molecular scale. *Sci. Reports* 7 (1): 2045–2322. doi:10.1038/s41598-017-16692-9.

McMurry, P. H. 2000. A review of atmospheric aerosol measurements. *Atmos. Environ.* 34 (12–14):1959–1999. doi:10.1016/S1352-2310(99)00455-0.

Merikanto, J., D. V. Spracklen, G. W. Mann, S. J. Pickering, and K. S. Carslaw. 2009. Impact of nucleation on global CCN. *Atmos. Chem. Phys.* 9 (21):8601–8616. doi:10.5194/acp-9-8601-2009.

Scheibel, H. G., and J. Porstendörfer. 1983. Generation of monodisperse Ag- and NaCl-aerosols with particle diameters between 2 and 300 nm. *J. Aerosol Sci.* 14 (2): 113–126. doi:10.1016/0021-8502(83)90035-6.

Schiesser, W. E., and C. A. Silebi. 1997. *Computational transport phenomena: Numerical methods for the solution of transport problems*. Cambridge, UK: Cambridge University Press.

Schobesberger, S.,. P. M. Winkler, T. Pinterich, A. Vrtala, M. Kulmala, and P. E. Wagner. 2010. Experiments on the temperature dependence of heterogeneous nucleation on nanometer-sized NaCl and Ag particles. *Chemphyschem* 11 (18):3874–3882. doi:10.1002/cphc.201000417.

Spracklen, D. V., K. S. Carslaw, M. Kulmala, V.-M. Kerminen, S.-L. Sihto, I. Riipinen, J. Merikanto, G. W. Mann, M. P. Chipperfield, A. Wiedensohler, W. Birmili, and H. Lihavainen. 2008. Contribution of particle formation to global cloud condensation nuclei concentrations. *Geophys. Res. Lett.* 35 (6):L06808. doi:10.1029/2007GL033038.

Stolzenburg, M. R., and P. H. McMurry. 1991. An ultrafine aerosol condensation nucleus counter. *Aerosol sci. Technol.* 14 (1):48–65. doi:10.1080/02786829108959470.

Stubenrauch, C., W. Rossow, S. Kinne, S. Ackerman, G. Cesana, H. Chepfer, L. Di Girolamo, B. Getzewich, A. Guignard, A. Heidinger, B. Maddux, W. Menzel, P. Minnis, C. Pearl, S. Platnick, C. Poulsen, J. Riedi, S. Sun-Mack, A. Walther, D. Winker, S. Zeng, and G. Zhao. 2013. Assessment of global cloud datasets from satellites: Project and database initiated by the gewex radiation panel. *Bull. Am. Meteorol. Soc.* 94 (7):1031–1049. doi:10.1175/BAMS-D-12-00117.1.

Takegawa, N., K. Iida, and H. Sakurai. 2017. Modification and laboratory evaluation of a tsi ultrafine condensation particle counter (model 3776) for airborne measurements. *Aerosol sci. Technol.* 51 (2):235–245. doi:10.1080/02786826.2016.1261990.

Tauber, C., X. Chen, P. E. Wagner, P. M. Winkler, C. J. Hogan, and A. Maißer. 2018. Heterogeneous nucleation onto monoatomic ions: Support for the Kelvin-Thomson theory. *ChemPhysChem* 19 (22):3144–3149. doi:10.1002/cphc.201800698.

Viisanen, Y., and R. Strey. 1994. Homogeneous nucleation rates for *n*butanol. *J. Chem. Phys.* 101 (9):7835–7843. doi:10.1063/1.468208.

Wagner, P. 1985. A constant-angle Mie scattering method (cams) for investigation of particle formation processes. *J. Colloid Interface Sci.* 105 (2):456–467. doi:10.1016/0021-9797(85)90319-4.

Wagner, P. E., D. Kaller, A. Vrtala, A. Lauri, M. Kulmala, and A. Laaksonen. 2003. Nucleation probability in binary heterogeneous nucleation of water-n-propanol vapor mixtures on insoluble and soluble nanoparticles. *Phys. Rev. E* 67 :021605. doi:10.1103/PhysRevE.67.021605.

Wiedensohler, A. 1988. An approximation of the bipolar charge distribution for particles in the submicron size range. *J. Aerosol Sci.* 19 (3):387–389. doi:10.1016/0021-8502(88)90278-9.

Wimmer, D., K. Lehtipalo, A. Franchin, J. Kangasluoma, F. Kreissl, A. Kürten, A. Kupc, A. Metzger, J. Mikkilä, T. Petäjä, F. Riccobono, J. Vanhanen, M. Kulmala, and J. Curtius. 2013. Performance of diethylene glycol-based particle counters in the Sub-3 nm size range. *Atmos. Measur. Tech.* 6 (7):1793–1804. doi:10.5194/amt-6-1793-2013.

Winkler, P. M., A. Hienola, G. Steiner, G. Hill, A. Vrtala, G. P. Reischl, M. Kulmala, and P. E. Wagner. 2008. Effects of seed particle size and composition on heterogeneous nucleation of n-nonane. *Atmos. Res.* 90 (2–4):187–194. doi:10.1016/j.atmosres.2008.02.001.

Winkler, P. M., R. L. McGraw, P. S. Bauer, C. Rentenberger, and P. E. Wagner. 2016. Direct determination of three-phase contact line properties on nearly molecular scale. *Sci. Reports* 6 :26111. doi:10.1038/srep26111.

Winkler, P. M., G. Steiner, A. Vrtala, H. Vehkamäki, M. Noppel, K. E. J. Lehtinen, G. P. Reischl, P. E. Wagner, and M. Kulmala. 2008. Heterogeneous nucleation experiments bridging the scale from molecular ion clusters to nanoparticles. *Science* 319 (5868):1374–1377. doi:10.1126/science.1149034.

Winkler, P. M., A. Vrtala, G. Steiner, D. Wimmer, H. Vehkamäki, K. E. J. Lehtinen, G. P. Reischl, M. Kulmala, and P. E. Wagner. 2012. Quantitative characterization of critical nanoclusters nucleated on large single molecules. *Phys. Rev. Lett.* 108 :085701. doi:10.1103/PhysRevLett.108.085701.